

1 **An ovine model for investigation of the microenvironment of the male mammary gland**

2

3 Benjamin P. Davies<sup>1</sup>, Rachael C. Crew<sup>2,3</sup>, Anna L. K. Cochrane<sup>2</sup>, Katie Davies<sup>2</sup>, Andre  
4 Figueiredo Baptista<sup>1</sup>, Sonja Jeckel<sup>4</sup>, Ian McCrone<sup>1</sup>, Youguo Niu<sup>2</sup>, Benjamin W. Strugnell<sup>5</sup>,  
5 Katie Waine<sup>5,6</sup>, Abigail L. Fowden<sup>2</sup>, Clare E. Bryant<sup>1</sup>, John W. Wills<sup>1</sup>, Dino A. Giussani<sup>2</sup>,  
6 Katherine Hughes<sup>1\*</sup>

7

- 8 1. Department of Veterinary Medicine, University of Cambridge, Cambridge, UK.  
9 2. Department of Physiology, Development and Neuroscience, University of Cambridge,  
10 Cambridge, UK.  
11 3. Department of Obstetrics and Gynaecology, University of Cambridge, UK.  
12 4. Farm Animal Pathology and Diagnostics, The Royal Veterinary College, Hatfield,  
13 UK.  
14 5. Farm Post Mortems Ltd, Durham, UK.  
15 6. Current address: Faculty of Veterinary Medicine, University of Calgary, Calgary, AB  
16 T3R 1J3, Canada.

17

18 \*Correspondence: Katherine Hughes, Department of Veterinary Medicine, University of  
19 Cambridge, Madingley Road, Cambridge, CB3 0ES, UK. Email [kh387@cam.ac.uk](mailto:kh387@cam.ac.uk)

20

21 **Running page heading**

22 Microenvironment of the male sheep mammary gland

23

24 **Abstract**

25

26 The specific biology of the male breast remains relatively unexplored in spite of the  
27 increasing global prevalence of male breast cancer. Delineation of the microenvironment of  
28 the male breast is restricted by the low availability of human samples and a lack of  
29 characterisation of appropriate animal models. Unlike the mouse, the male ovine gland  
30 persists postnatally. We suggest that the male ovine mammary gland constitutes a promising  
31 adjunctive model for the male human breast. In this study we evaluate the male ovine  
32 mammary gland microenvironment, comparing intact and neutered males. Assessment of the  
33 glandular histo-anatomy highlights the resemblance of the male gland to that of the neonatal  
34 female sheep and confirms the presence of rudimentary terminal duct lobular units.

35 Irrespective of neutered status, cell proliferation in epithelial and stromal compartments is  
36 low in males, and cell proliferation in epithelial cells and in the intralobular stroma is  
37 significantly lower than in pubertal female sheep. Between 42% and 72% of the luminal  
38 mammary epithelial cells in the male gland express the androgen receptor, and expression is  
39 significantly reduced by neutering. Luminal epithelial cells within the intact and neutered  
40 male gland also express oestrogen receptor alpha, but minimal progesterone receptor  
41 expression is observed. The distribution of mammary leukocytes within the ducts and stroma  
42 is similar in the female mammary gland of sheep and other species. Both macrophages and T  
43 lymphocytes are intercalated in the epithelial bilayer and are more abundant in the  
44 intralobular stroma than the interlobular stroma, suggesting that they may have a protective  
45 immunological function within the vestigial glandular tissue of the male sheep. Mast cells are  
46 also observed within the stroma. These cells cluster nearer the glandular tissue and are  
47 frequently located adjacent to blood vessels. The abundance of mast cells is significantly  
48 higher in intact males compared to neutered males, suggesting that hormone signalling may  
49 impact mast cell recruitment. In this study, we demonstrate the utility of the male ovine

50 mammary gland as a model for furthering our knowledge of postnatal male mammary  
51 biology.

52

53 **Keywords**

54 Male; mammary gland; microenvironment; model; sheep; udder

55

56

57 **Introduction**

58 The mammary gland nourishes and supports the development of offspring. Whilst they are  
59 intrinsically linked with female individuals, mammary glands persist in the majority of male  
60 mammals, although with notable exceptions including mice, horses and marsupials (Cardiff  
61 et al., 2018; Hughes, 2021a; Renfree et al., 1990).

62

63 Early fetal development of the male mammary gland is typically consistent with that of the  
64 female, irrespective of species (Hassiotou and Geddes, 2013; Jenkinson, 2003; Pokharel et  
65 al., 2018). Between embryonic day 11 and 13 of fetal mouse development, mammary  
66 placodes are established from ectoderm thickening on bilateral milk lines (Macias and Hinck,  
67 2012; Stewart et al., 2019). The mammary placodes then invaginate into the mesenchyme  
68 layer, forming mammary buds (Paine and Lewis, 2017). Sexual dimorphism of the mouse  
69 mammary gland is established at embryonic day 14 (Richert et al., 2000; Stewart et al.,  
70 2019). In male mice, androgen is produced from the developing testes which causes  
71 condensation of the mesenchyme within the developing mammary gland (Dürnberger and  
72 Kratochwil, 1980; Richert et al., 2000; Vandenberg et al., 2013). This results in the  
73 morphological distortion of the mammary epithelium detaching the gland from the overlying  
74 epidermis (Drews and Drews, 1977; Richert et al., 2000; Stewart et al., 2019). The gland  
75 thereafter regresses and at birth comprises minimal vestigial glandular tissue that lacks  
76 nipples (Cardiff et al., 2018; Pokharel et al., 2018; Szabo and Vandenberg, 2021). In some  
77 genetically modified mouse strains, glandular tissue can persist after birth (Pokharel et al.,  
78 2018; Szabo and Vandenberg, 2021) but may still lack key developmental structures required  
79 for mammary gland expansion such as terminal end buds (Kolla et al., 2017).

80

81 By contrast, human prepubescent breast development is consistent between the sexes until the  
82 influence of androgen at puberty limits both ductal and stromal expansion of male breast  
83 tissue (Hassiotou and Geddes, 2013; Jesinger, 2014). The male breast comprises a small  
84 arborising ductal tree, apparently largely without well-developed lobules, embedded in an  
85 adipose-rich stroma (Fox et al., 2022).

86

87 The male breast has the potential to develop similar pathologies to that of females but at a  
88 lower incidence (Chatterji et al., 2023; Iuanow et al., 2011). However, there has been less  
89 focus on the specific biology of the male breast. Prevalence of male breast cancer is  
90 increasing globally (Fox et al., 2022) and the risk of death is significantly higher than  
91 comparable female breast cancers (Liu et al., 2018). Male breast neoplasms also have  
92 different biology compared to breast neoplasms arising in women (Chatterji et al., 2023).

93 Research focussed specifically on the male breast is currently limited by both the low  
94 availability of human samples and the lack of characterisation of appropriate animal models  
95 in which the complete male mammary structure persists postnatally.

96

97 Sheep are commonly used to model human fetal development (Morrison et al., 2018) and we  
98 and others have noted anatomical similarities in mammary terminal duct lobular unit (TDLU)  
99 structure and stromal composition between the sheep mammary gland and the female breast  
100 (Hovey et al., 1999; Hughes, 2021b; Hughes and Watson, 2018; Nagy et al., 2021; Rowson et  
101 al., 2012). Male and female ovine fetuses exhibit parallel mammary developmental, with the  
102 gland and teat cistern present in both sexes around fetal day 80 (Jenkinson, 2003). However,  
103 there has been little examination of the male ovine mammary gland postnatally. We suggest  
104 that the mammary gland of the male sheep may constitute a promising model of the male

105 human breast. Consequently, in this study we evaluate the mammary microenvironment in the  
106 male sheep, comparing intact and neutered males to highlight how male specific sex  
107 hormones may affect the mammary microenvironment.

108

109 **Materials and Methods**

110 *Animals*

111 Ovine mammary tissue was obtained from both male and female sheep that were submitted to  
112 the diagnostic veterinary anatomic pathology services of either the Department of Veterinary  
113 Medicine, University of Cambridge or to the Royal Veterinary College. Mammary tissue was  
114 also collected during the post mortem examination of Welsh mountain sheep, euthanised for  
115 research purposes under the Animals (Scientific Procedures) Act 1986. The Ethics and  
116 Welfare Committee of the Department of Veterinary Medicine, University of Cambridge,  
117 approved the study plan to use post mortem tissue in this project (references: CR223 and  
118 CR625). The nonregulated scientific use of post mortem mammary tissue collected from  
119 research animals was approved by the Named Veterinary Surgeon of the University of  
120 Cambridge. Any tissue containing evidence of mammary pathology was excluded from the  
121 study.

122

123 Male sheep used in this study ranged from 3 days old to 3 years old, but only animals older  
124 than 4 months were included in quantification analysis. Pubertal female sheep were aged  
125 from 4 months to 11 months. Mature female sheep were all older than two years and were not  
126 expected to be oestrus cycling based on the time of year of the post mortem examination  
127 (sheep are seasonal breeders). The sheep used were from a variety of breeds (Supplementary  
128 Table 1).

129

130 *Tissue processing*

131 Mammary tissue was fixed in 10% neutral-buffered formalin for approximately one week.  
132 The entire male mammary gland and samples of female mammary parenchyma were then  
133 trimmed, processed using a routine histology protocol and embedded in paraffin. Sections  
134 were cut at 5 µm and mounted on coated glass slides (TOMO®) or stained with haematoxylin  
135 and eosin to check for microscopic pathology prior to inclusion in the study.

136

137 *Dual immunohistochemistry and immunofluorescence*

138 Formalin fixed paraffin embedded (FFPE) tissue was subjected to antigen retrieval using a PT  
139 link module and high pH antigen retrieval solution (both Dako Pathology/Agilent  
140 Technologies, Stockport, UK). For dual immunohistochemistry, an ImmPRESS® Duet  
141 Double Staining Polymer Kit (Vector Laboratories) was used. Primary antibodies were added  
142 at the appropriate concentration (Supplementary Table 2) and incubated overnight at 4°C.  
143 Negative controls received isotype- and species-matched immunoglobulins. Counterstaining  
144 was achieved by incubating in Mayer's Haematoxylin for 4 minutes. Slides were dehydrated  
145 in an ethanol and xylene series and Pertex® Mounting Medium was added dropwise.  
146 ClariTex Coverslips (24 x 50mm) were then applied.

147

148 For immunofluorescence, slides were first incubated with 10% normal goat serum for 1 hour  
149 at room temperature. Primary antibodies were added at the appropriate concentration  
150 (Supplementary Table 2) and incubated overnight at 4°C. Slides were then incubated in  
151 darkness with secondary antibodies (Supplementary Table

152 2) for 1 hour at room temperature. Negative controls received isotype- and species-matched  
153 immunoglobulins. Nuclei staining was performed by incubating with DAPI (10.9  $\mu$ M)  
154 (SigmaAldrich/Merck Life Science UK Limited, Gillingham, UK) for 5 minutes. Slides were  
155 cover-slipped using Vectashield® VibranceTM Antifade mounting medium (catalogue H-  
156 1700; Vector laboratories, Peterborough, UK) and imaged using a Leica TCS SP8 confocal  
157 microscope.

158

159 *Clear, unobstructed brain imaging cocktails (CUBIC)*

160 Mammary tissue was dissected and fixed in 10% neutral-buffered formalin for 6 to 26 hours.  
161 The gland was trimmed into smaller samples, approximately 15 x 15 x 5 mm. These samples  
162 were optically cleared using the CUBIC protocol (Lloyd-Lewis et al., 2016; Susaki et al.,  
163 2014) with the modifications outlined below. Tissue was incubated in CUBIC reagent 1A for  
164 4 days on a shaker at 37°C. The solution was replaced daily. Samples were then incubated  
165 overnight, on a shaker at 4°C, with a blocking solution containing normal goat serum [10%  
166 (volume per volume)] and Triton X-100 [0.5% (weight per volume)] in phosphate-buffered  
167 saline (PBS). Primary antibodies, diluted in blocking solution, were applied at appropriate  
168 concentrations (Supplementary Table 2) and samples were incubated for 4 days on a shaker at  
169 4 °C. Tissue samples were subsequently thoroughly washed in PBS and secondary antibodies  
170 (Supplementary Table 2), also diluted in blocking solution, were then applied. Samples were  
171 incubated in darkness on a shaker at 4 °C. Negative controls received isotype- and species-  
172 matched immunoglobulins. After further washing in PBS containing Triton X-100 (0.1%  
173 (weight per weight)), nuclei staining was performed by incubating in DAPI (10.9  $\mu$ M)  
174 (SigmaAldrich/Merck Life Science UK Limited, Gillingham, UK) at room temperature for at  
175 least 1 hour. After further washing, CUBIC reagent 2 was applied and incubated in darkness

176 for 4 days on shaker at 37 °C. Tissue samples were imaged in Ibidi 35 mm glass bottom  
177 dishes (catalogue 81218-200; ibidi GmbH, Gräfelfing, Germany) using a Leica TCS SP8  
178 confocal microscope.

179

180 *Slide scanning*

181 Slides subjected to immunohistochemical staining were scanned at 40× magnification using a  
182 NanoZoomer 2.0RS, C10730, (Hamamatsu Photonics, Hamamatsu City, Japan). Scanned  
183 sections were analysed with viewing software (NDP.view2, Hamamatsu Photonics).

184

185 *Sampling for cell proliferation and immune cell abundance*

186 Slide scans were analysed with NDP.view2 viewing software. Depending on the tissue area  
187 available for analysis, three to eight count boxes (400 × 230 µm) were randomly placed on  
188 each slide at 1.25x magnification. Boxes containing artefacts from slide cutting or scanning  
189 were repositioned.

190

191 *Quantification of epithelial and stromal proliferation*

192 Instances of myoepithelial and luminal cell proliferation, and proliferation of any cells  
193 located within the interlobular and intralobular stroma, as denoted by positive nuclear Ki67  
194 staining, were manually counted. The total count for all sample boxes on the slide was  
195 calculated. This total count was then normalised to the total sampled area (mm<sup>2</sup>) of glandular  
196 tissue, interlobular or intralobular stroma, calculated by tracing around the area using the  
197 NDP.view2 freehand annotation tool. The protocol was repeated for all individuals within  
198 each experimental group and the mean was derived.

199

200 *Manual quantification of hormone receptor expression*

201 A Leica TCS SP8 confocal microscope was utilised to produce x400 magnification tile scans  
202 of immunofluorescence slides. Tile scans were analysed using Fiji (Schindelin et al., 2012),  
203 and, depending on the size of the tissue, three to eight count boxes (each measuring 400 ×  
204 230  $\mu\text{m}$ ) were randomly placed on each slide at low magnification. Hormone receptor  
205 positive luminal epithelial cell nuclei were manually counted and the total count for all  
206 sample boxes on the slide was calculated. This count was expressed as a percentage of the  
207 total number of luminal epithelial cell nuclei within all sample count boxes. The protocol was  
208 repeated for all individuals within each experimental group and the mean percentage of  
209 hormone receptor positive luminal cell nuclei for each group was calculated.

210

211 *Epithelial and Stromal Macrophage and T lymphocyte abundance*

212 Using NDP.view2, the number of epithelial-associated IBA1 positive-macrophages and CD3-  
213 positive T lymphocytes were counted. Cells were considered epithelial-associated if >50% of  
214 their cytoplasmic perimeter contacted the basement membrane. The total number of  
215 epithelial-associated macrophages and T lymphocytes in all count boxes was calculated for  
216 each individual, together with the total number of epithelial cells, and the epithelial-  
217 associated immune cell count was expressed per 100 luminal epithelial cells. Stromal  
218 macrophages and T lymphocytes were considered to be interlobular and intralobular  
219 respectively when >50% of their cytoplasmic perimeter was within the respective type of  
220 stroma. The total number of macrophages and T lymphocytes for each stroma type was  
221 calculated. This count was normalised to the total sampled area ( $\text{mm}^2$ ) of interlobular or

222 intralobular stroma, determined using the NDP.view2 freehand annotation tool. The protocol  
223 was repeated for all individuals within each experimental group and the mean was derived.

224

225 *Statistical analysis*

226 To assess statistical significance in comparisons between cell proliferation and comparisons  
227 between hormone receptor expression, a Kruskal-Wallis test was conducted. Statistical  
228 significance in the differences in immune cell abundance between intact and neutered males  
229 were assessed using a Mann-Whitney U test. To assess statistical significance in the  
230 differences in immune cell abundance between intra- and interlobular stroma, a Wilcoxon  
231 signed-rank test was performed. All data were collected using Microsoft Excel and were  
232 analysed using R studio (RStudio: Integrated Development for R. RStudio, PBC, Boston, MA  
233 URL <http://www.rstudio.com/>). All data are presented as mean values + the standard  
234 deviation.

235

236 **Results and Discussion**

237 *The gross and histo-anatomy of the male sheep mammary gland resembles that of the  
238 neonatal female.*

239 In total, thirty-three sheep were analysed in the study (Suppl. Table 1) Nineteen of these  
240 sheep were male, comprising eight intact males and eleven neutered males. These male sheep  
241 ranged between three days old to three years old, but only male sheep older than four months  
242 were included in analyses involving quantification. These male sheep were of several  
243 different breeds, including four Cheviot cross males, three Welsh mountain males, three Texel  
244 cross males and one of each of Jacob cross, New Zealand Romney, Suffolk, Mule, Mule cross

245 and Shetland. For three male sheep no breed information was available. Male sheep were  
246 compared to a group of seven pubertal female sheep and seven mature female ewes. Pubertal  
247 females ranged from four to eleven months in age. These ewes were of three different breeds  
248 comprising five Welsh mountain ewes and one each of Texel cross and Beltex. Mature  
249 females were all older than two years and all seven were Welsh mountain ewes.

250

251 To investigate the possibility that the mammary gland of the male sheep is a useful adjunct  
252 model for the male breast, we initially characterised the gross and histo-anatomy of the gland.  
253 The male sheep mammary gland is located in the sub-epithelial tissues below the teat (Fig. 1  
254 a) and is composed of branching ducts that terminate in terminal duct lobular units (TDLUs)  
255 (Fig. 1 b-e). The walls of the ducts comprise a bilayer of luminal epithelial cells and basal  
256 myoepithelial cells (Fig. 1 b). Both intra- and interlobular mammary stroma surrounds the  
257 ductal system (Fig. 1 c) and, like that of the female ruminant, expresses smooth muscle actin  
258 (Nagy et al., 2021; Safayi et al., 2012). Overall the structure of the male gland is very similar  
259 to that of the neonatal female sheep (Hughes, 2021b; Nagy et al., 2021) and contrasts the  
260 minimal vestigial glandular tissue present in the postnatal male mouse mammary gland  
261 (Cardiff et al., 2018; Pokharel et al., 2018; Stewart et al., 2019; Szabo and Vandenberg,  
262 2021).

263

264 *The male ovine mammary gland exhibits minimal cell proliferation, irrespective of neutered*  
265 *status.*

266 Given that the female mammary gland undergoes dynamic changes in cell proliferation  
267 throughout its postnatal development cycle (Inman et al., 2015) we wished to assess the  
268 proliferation dynamics of different cellular compartments within the male gland, comparing

269 intact and neutered male animals with pubertal females and mature females. Proliferation in  
270 both epithelial and stromal compartments is similarly low in male sheep irrespective of neuter  
271 status. Proliferation in luminal epithelial cells, myoepithelial cells and cells present in the  
272 intralobular stroma, is significantly higher in pubertal females when compared to both intact  
273 and neutered males (Fig 2 e-g).

274

275 *Neutering decreases mammary androgen receptor expression in sheep.*

276 In our study population, between 42% and 72% of luminal mammary epithelial cells in intact  
277 male sheep express androgen receptor (AR) and expression is abrogated by neutering (Fig.  
278 3). Previously studies have illustrated that androgen receptor activation limits the expansion  
279 of glandular tissue within the female mammary gland. Transgenic mouse models in which the  
280 production or action of AR was ablated, exhibited increased cell proliferation, ductal  
281 branching and number of terminal end buds (Gao et al., 2014; Simanainen et al., 2012). In  
282 humans, AR functions to limit the growth of breast tissue in both prepubescent boys and girls  
283 (Dimitrakakis and Bondy, 2009), and our data in the sheep are consistent with this  
284 observation.

285

286 Oestrogen receptor alpha (ER alpha) expression has previously been highlighted in epithelial  
287 cells within the TDLUs of prepubertal sheep (Colitti and Parillo, 2013) and is similarly  
288 observed in both male and female groups in our study (Fig. 3e- 3h). Our analysis indicates  
289 that intact males have a higher percentage of luminal epithelial cells exhibiting ER alpha  
290 expression than mature females (Fig. 3n), potentially reflecting a variable composition of  
291 luminal epithelial sub-groups in the male gland compared to the female. Understanding the  
292 balance between AR and ER alpha expression in the male mammary gland is important

293 because the vast majority of male breast cancer is ER positive (Cardoso et al., 2018; Chatterji  
294 et al., 2023).

295

296 Mean progesterone receptor expression is higher in pubertal females than neutered males  
297 (Fig. 3o). Progesterone receptor expression has been previously reported in the alveolar cells  
298 of the female ovine mammary gland during lactation (Colitti and Parillo, 2013) and prior  
299 research, using hormone treated murine mammary glands, indicates that progesterone  
300 receptor signalling promotes ductal branching during puberty (Atwood et al., 2000).  
301 Progesterone receptor signalling has also been shown to promote cell proliferation in multiple  
302 mammary cell types during puberty and pregnancy (Atwood et al., 2000; Brisken et al., 1998;  
303 Hilton et al., 2015). The low expression of progesterone receptor in neutered males and low  
304 but variable levels of progesterone receptor expression in intact males are consistent with the  
305 relatively limited tissue area occupied by the male gland and the lack of cell proliferation we  
306 observe within the male mammary gland (Fig. 2e-2h).

307

308 *Macrophages and T lymphocytes are intercalated in the epithelial bilayer and cluster nearer*  
309 *ductal structures in the male ovine mammary gland.*

310 In both intact and neutered male sheep, IBA-1 positive macrophages are intercalated in the  
311 epithelial bilayer and are present in the intra- and interlobular mammary stroma. There are  
312 abundant macrophages surrounding the TDLUs and many are intimately associated with the  
313 epithelium (Fig. 4). The localisation of mammary macrophages in the male sheep is overall  
314 consistent with previous characterisation of the female neonatal and pubertal ovine mammary  
315 gland, with the exception that the macrophages within the male gland do not appear to exhibit  
316 the periodicity previously noted in females (Nagy et al., 2021). The intraepithelial

317 macrophages of the male gland may be similar to the ductal macrophages reported in the  
318 mouse mammary gland (Dawson et al., 2020). These ductal macrophages have phenotypes  
319 and gene expression patterns distinct from stromal macrophages, reflecting an immune  
320 surveillance function (Dawson et al., 2020). The macrophages within the male ovine gland  
321 could have a similar role, but their precise phenotype and function requires further  
322 elucidation. In female mice, macrophage abundance also is affected by oestrogen and  
323 progesterone, during oestrus cycling (Chua et al., 2010; Hodson et al., 2013; Tower et al.,  
324 2022) and macrophages are receptive to androgen signalling (Liva and Voskuhl, 2001).  
325 However, our data suggest that male ovine mammary gland macrophage abundance is  
326 unaffected by neutered status (Suppl. Fig 1), an observation warranting further future  
327 investigation.

328

329 In both intact and neutered males, the abundance of macrophages is significantly higher in  
330 the intralobular stroma, directly surrounding the glandular tissue, compared to the more  
331 distant interlobular stroma (Fig. 4). This is consistent with previous examination of the  
332 female bovine mammary gland (Beaudry et al., 2016).

333

334 Similar to epithelial-associated macrophages, CD3 positive T lymphocytes are intercalated in  
335 the epithelial bilayer and are present in the intra- and interlobular mammary stroma. In  
336 contrast, there are few CD20-positive B lymphocytes (Fig. 5). Comparisons between intact  
337 and neutered males highlight that there is no significant difference in abundance of T  
338 lymphocytes associated with the epithelium or in the intra- or interlobular stroma (Suppl. Fig.  
339 2). In neutered males there are more T lymphocytes in the intralobular stroma than in the  
340 interlobular stroma (Fig. 5). The clustering of both macrophages and T lymphocytes within

341 and near the male mammary ductal structures may imply that they have an active  
342 immunological function with the male ovine vestigial glandular tissue, which has a potential  
343 portal for ingress of pathogens from the exterior through the teat.

344

345 *Mast cells cluster nearer ductal structures in the male ovine mammary gland and their*  
346 *abundance is significantly higher in intact males.*

347 Mast cells have been previously identified in the mammary gland of the mouse (Hughes et  
348 al., 2012; Lilla and Werb, 2010), rat (Ramirez et al., 2012) and cow (Beaudry et al., 2016).  
349 Typically, histological identification of mast cells is carried out using toluidine blue staining  
350 to highlight the cells' metachromatic staining granules. We and others have used toluidine  
351 blue to identify mast cells in the mammary gland of laboratory rodents (Hughes et al., 2012;  
352 Lilla and Werb, 2010; Ramirez et al., 2012). However, toluidine blue staining does not  
353 positively stain mast cells in the ovine mammary gland, potentially due to differences in  
354 granule composition (Suppl. Fig. 3). Consequently, we have stained for c-Kit, a  
355 transmembrane tyrosine kinase receptor (Ribatti, 2018), that has been previously used to  
356 identify mast cells in human tissues (Lammie et al., 1994). Mast cells are present in the  
357 mammary stroma in both intact and neutered male glands and are present in close proximity  
358 to blood vessels (Fig. 6). This localisation is consistent with previous descriptions of mast  
359 cells in the female mouse mammary gland (Lilla and Werb, 2010).

360

361 The abundance of mast cells in the intra- and interlobular stroma is significantly higher in  
362 intact males compared to neutered males (Fig. 6d - e), suggesting that steroid hormone  
363 signalling may impact mast cell recruitment. A prior study highlighted that mast cells within  
364 the human skin express androgen receptors, but mast cell degranulation remained unchanged

365 upon the administration of a testosterone treatment (Chen et al., 2010). However, authors did  
366 not comment how testosterone treatment may have affected mast cell abundance. There is  
367 also some evidence that oestrogen could affect mast cell recruitment in the female bovine  
368 mammary gland, where researchers identified a trend in which that mast cell number  
369 increases upon the exogenous oestrogen treatment (Beaudry et al., 2016). Elucidating how  
370 specific hormone receptor signalling may affect mast cell recruitment within the male ovine  
371 gland is a direction for further experimental investigation.

372

373 Consistent with the analysis of macrophage and T lymphocyte abundance, mast cell  
374 abundance is also significantly higher in the intralobular stroma, compared to the more  
375 distant interlobular stroma (Fig. 6f - g). This is seen in both intact and neutered males.  
376 Similarly in the rat mammary gland mast cells tend to be located in the stroma surrounding  
377 the ducts (Ramirez et al., 2012). Mast cell number is also four times higher in the stroma  
378 adjacent to the mammary ducts, compared to more distant regions, in the female bovine  
379 mammary gland (Beaudry et al., 2016). This suggests that mammary mast cell localisation is  
380 similar between species and between males and females.

381

382 *Conclusions*

383 The ovine tissue analysed in this study was obtained from multiple sources from sheep with  
384 different genetic backgrounds and maintained with different husbandry practices.  
385 Additionally, tissue obtained from pubertal females was collected from sheep euthanised  
386 throughout the year and their stage of the oestrus cycle at the time of tissue collection is  
387 unknown. Together, this constitutes a heterogeneous sample population which introduces

388 considerable variability into the dataset. Arguably, this mirrors the heterogeneity in the  
389 mammary microenvironment in the human population.

390

391 This study demonstrates the utility of the male ovine mammary gland as a tool to further our  
392 understanding of postnatal male mammary biology. This vestigial glandular structure contains  
393 a diverse set of immune cell types and exhibits distinct hormone receptor expression patterns,  
394 features that in both cases are affected by neutered status. Interestingly, the immune  
395 microenvironment of the male ovine gland appears to share features with that of the female  
396 gland in sheep and other species. This observation, together with the well-documented histo-  
397 anatomical similarities of the sheep mammary gland to the human breast (Hughes, 2021b;  
398 Nagy et al., 2021; Rowson et al., 2012) indicate that the male sheep mammary gland may be  
399 a useful adjunctive model of the male human breast. As mammary tumourigenesis is rare in  
400 sheep (Hughes, 2021b; Newman et al., 2021), the male ovine gland does not offer a direct  
401 model for male breast cancer, but it will facilitate furthering understanding of normal male  
402 mammary biology to use in comparative studies. In addition, the relative resistance of the  
403 sheep to development of mammary tumours may be a further fruitful avenue of future  
404 comparative study (Hughes, 2023).

405

#### 406 **Acknowledgements**

407 BPD is supported by an Anatomical Society PhD studentship awarded to KH. The authors  
408 would like to thank Hugh Balmer, Yvonne Pratt, Andrea Starling and Emma Ward of the  
409 Department of Veterinary Medicine, University of Cambridge, for their excellent technical  
410 expertise in the preparation of tissue sections, and Mathew Rhodes, of the same department,  
411 for technical assistance in the post mortem room. We acknowledge the Ethics and Welfare

412 Committee of the Department of Veterinary Medicine, University of Cambridge, for their  
413 review of the study plan relating to the use of tissue from ovine post mortem examinations for  
414 the study of mammary gland biology (references: CR223 and CR625). Parts of this data were  
415 presented in oral abstract form at the European Network for Breast Development and  
416 Cancer online seminar series (presentation date 6 December 2022) and at the Anatomical  
417 Society Summer Meeting 2023 in Bangor, Wales (25-27 July 2023; presentation date 25 July  
418 2023).

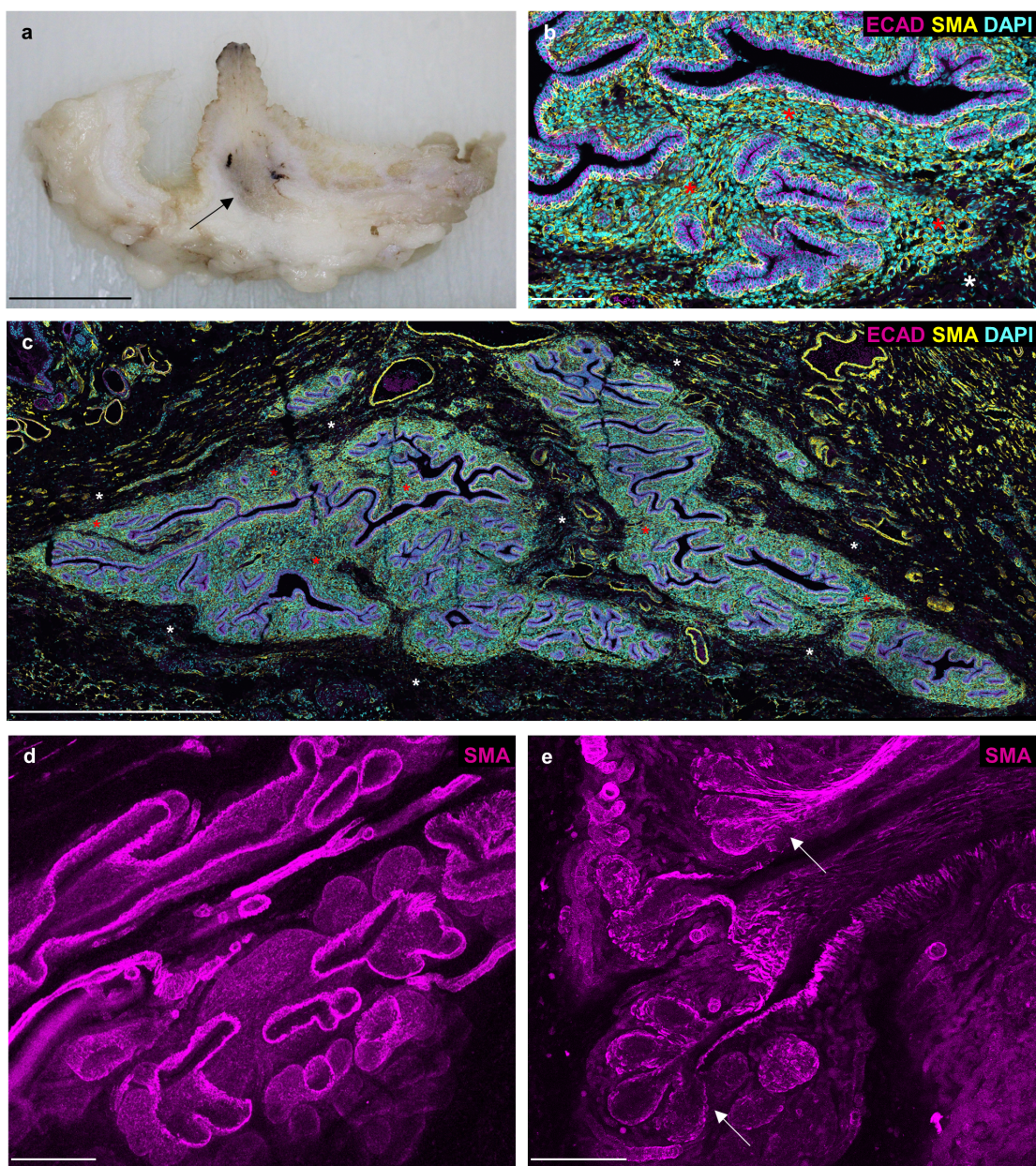
419

420 **Author contributions**

421 BPD and KH contributed to study concept and design. BPD, RCC, ALKC, KD, AFB, SJ, IM,  
422 YN, BWS, KW, ALF, DAG and KH contributed to acquisition of data. BPD, CEB, JWW, and  
423 KH contributed to data analysis and interpretation. BPD and KH drafted the manuscript. All  
424 authors contributed to critical revision of the manuscript and approved the final version.

425

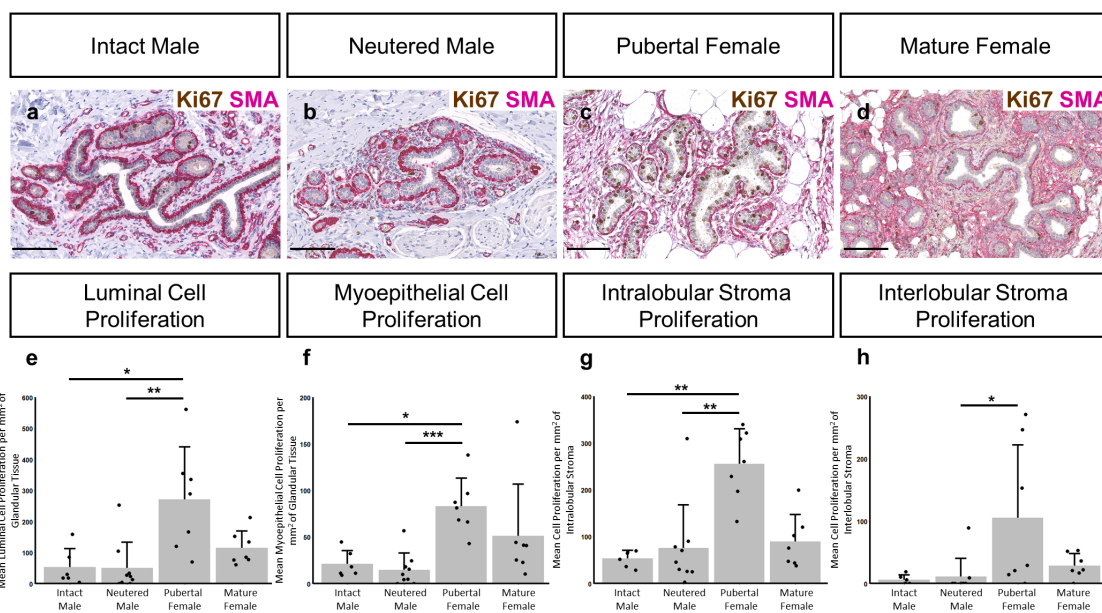
426 **Figures**



427

428 **Figure 1: Macro and histo-anatomy of the male ovine mammary gland. (a)** A sub-gross  
429 image of fixed male ovine mammary tissue. Arrow indicates mammary gland. **(b, c)**  
430 Immunofluorescence staining for luminal epithelial cells, using E-cadherin (magenta),  
431 myoepithelial cells, using alpha-smooth muscle actin (yellow) and DNA, using DAPI (cyan).  
432 Red asterisks indicate areas of intralobular mammary stroma. White asterisks indicate areas  
433 of interlobular mammary stroma. **(d, e)** 3D maximum intensity projections of optically

434 cleared male ovine mammary tissue, using confocal microscopy. Immunofluorescence  
435 staining for alpha-smooth muscle actin (magenta). Arrows indicate terminal duct lobular  
436 units. Images are representative of 3 biological repeats Scale bar = 1 cm (**a**); 100  $\mu$ m (**b**); 1  
437 mm (**c**); 200  $\mu$ m (**d**); 100  $\mu$ m (**e**).



438

439 **Figure 2: Proliferation dynamics within the intact male, neutered male, pubertal female**  
440 **and mature female mammary gland. (a-d)** Dual immunohistochemical staining for Ki67  
441 (brown) and alpha-SMA (magenta) in the mammary gland of intact males (a), neutered males  
442 (b), pubertal females (c) and mature females (d). (e-h) Bar graphs illustrating differences in  
443 mean luminal cell proliferation (e), myoepithelial cell proliferation (f), intralobular stroma  
444 proliferation (g) and interlobular stroma proliferation (h) per mm<sup>2</sup> of glandular tissue, intra-  
445 or interlobular mammary stroma + standard deviation (\*p < 0.05, \*\*p < 0.01, \*\*\*p < 0.001, N=

446 6 for intact males, N = 9 for neutered males, N= 7 for pubertal females, N = 7 for mature

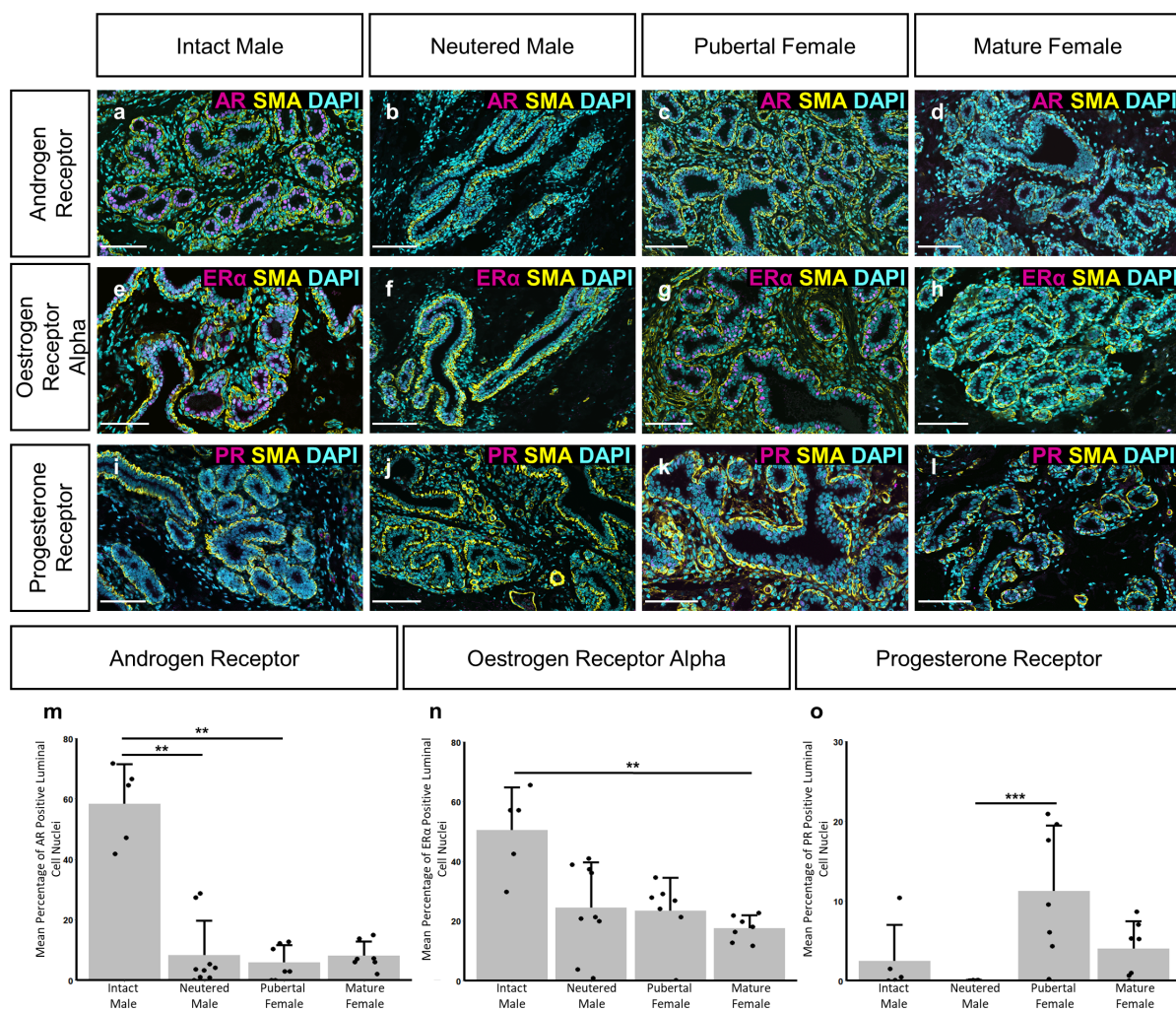
447 females, using Kruskal-Wallis test). Dots represent individual sheep. Images representative of

448 6 (a), 9 (b) and 7 (c, d) biological repeats. All IHC shown with a haematoxylin counterstain.

449 Scale bar = 100 µm (a-d).

450

451



452

453 **Figure 3: Differences in mammary epithelial hormone receptor expression between**

454 **intact males, neutered males, pubertal females and mature females. (a-l)**

455 Immunofluorescence staining for androgen receptor (AR) (a-d), oestrogen receptor alpha

456 (ER $\alpha$ ) (e-h), progesterone receptor A/B (PR) (i-l) (magenta), alpha-SMA (yellow) and DAPI

457 (cyan) in the mammary gland of intact males (a, e, i), neutered males (b, f, j), pubertal

458 females (c, g, k) and mature females (d, h, l). (m-o) Bar graphs illustrating differences in the

459 mean percentage of AR (m), ER $\alpha$  (n) or PR (o) positive luminal cell nuclei + standard

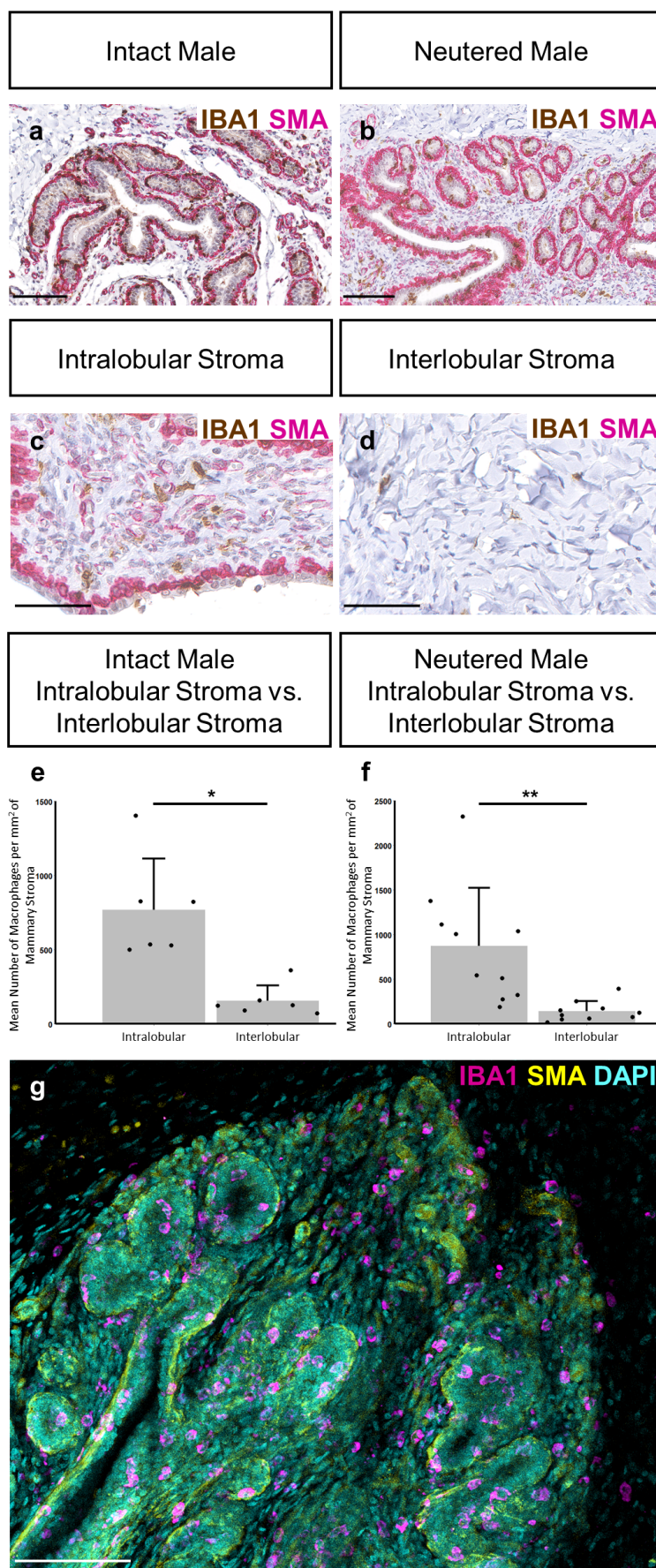
460 deviation (\*\*p< 0.01, \*\*\*p< 0.001, N= 5 for intact males, N =9 for neutered males, N= 7 for

461 pubertal females, N = 7 for mature females, using Kruskal-Wallis test). Dots represent

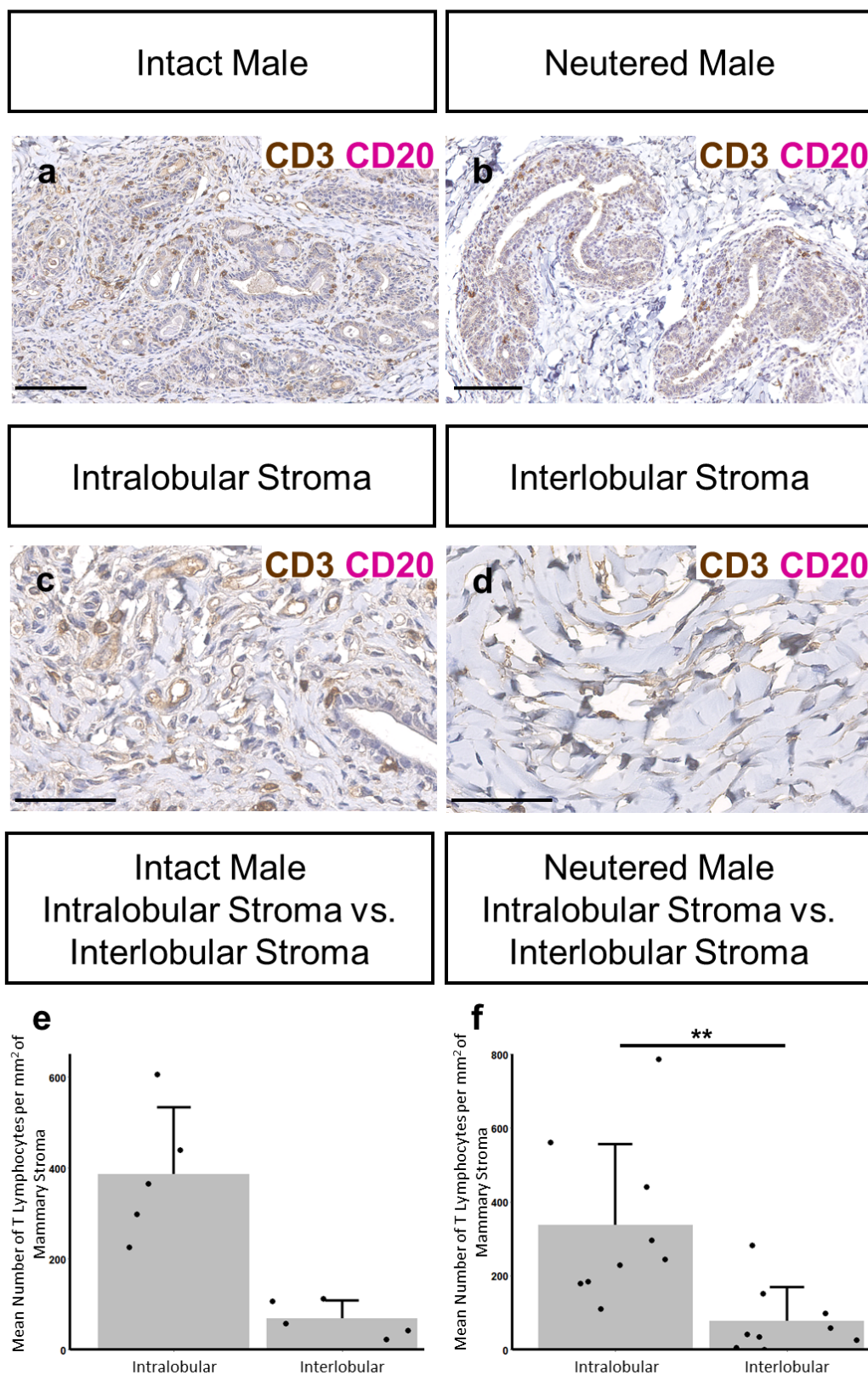
462 individual sheep. Images representative of 5 (**a, e, i**), 9 (**b, f, j**) and 7 (**c, d, g, h, k, l**)

463 biological repeats. Scale bar = 100  $\mu\text{m}$  (**a-l**).

464



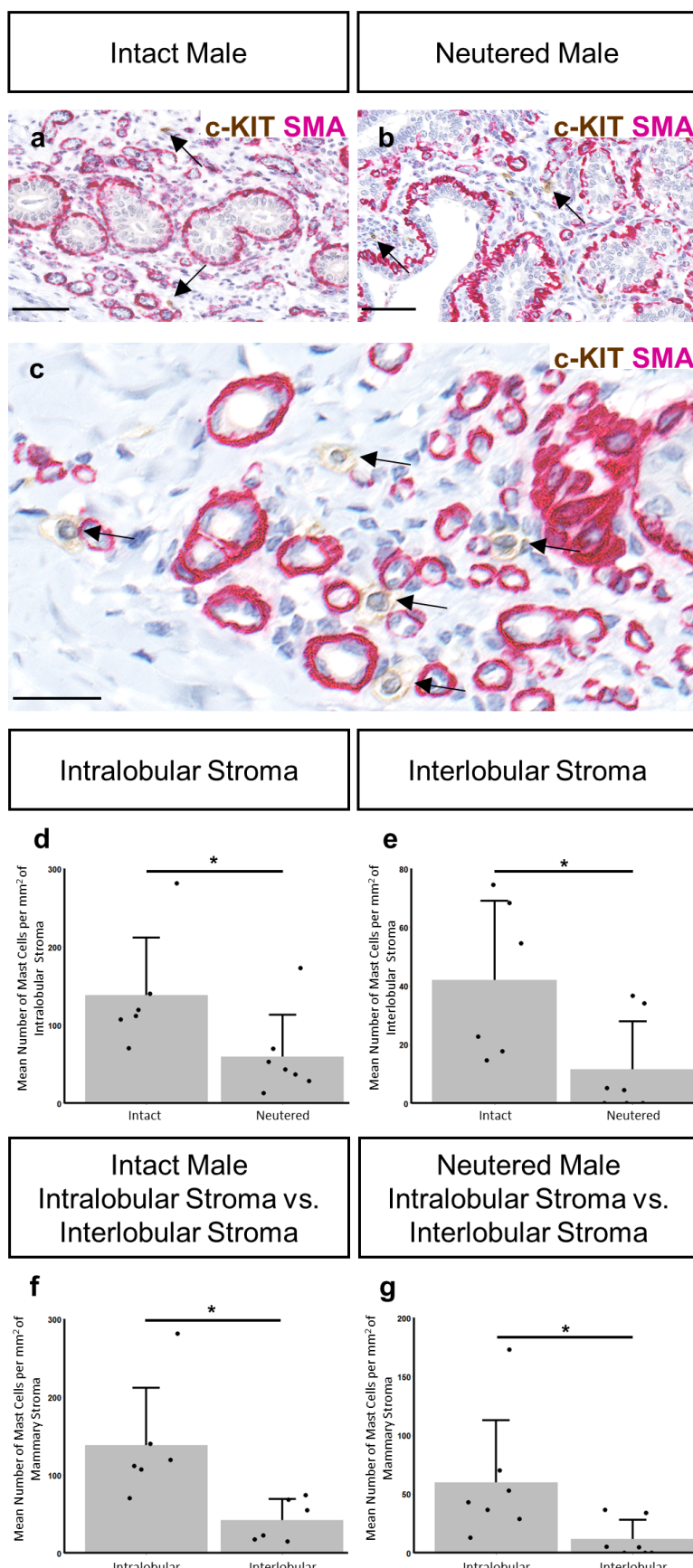
466 **Figure 4: Macrophage abundance and localisation within the intact and neutered male**  
467 **ovine mammary gland. (a-d)** Dual immunohistochemical staining for IBA1 (brown) and  
468 alpha-SMA (magenta) in the mammary gland of intact males (a) and neutered males (b). (c-  
469 d) The abundance of macrophages in the intralobular (c) and interlobular mammary stroma  
470 (d). (e, f) Bar graphs illustrating differences in the mean number of macrophages per mm<sup>2</sup> of  
471 mammary stroma in the intralobular and interlobular stroma of intact (e) and neutered males  
472 (f) + standard deviation (\*p< 0.05, \*\*p< 0.01, N= 6 for intact males, N =10 for neutered  
473 males, using Wilcoxon signed-rank test). Dots represent individual sheep. (g) A 3D maximum  
474 intensity projection of optically cleared male ovine mammary tissue, using confocal  
475 microscopy. Immunofluorescence staining for IBA1 (magenta), alpha-SMA (yellow) and  
476 DAPI (cyan). Images representative of 6 (a), 10 (b, c, d) and 3 (g) biological repeats. Scale  
477 bar = 100 µm (a, b, g); 50 µm (c, d).



479 **Figure 5: T- lymphocyte abundance within the intact and neutered male ovine**  
480 **mammary gland. (a-d)** Dual immunohistochemical staining for CD3 (brown) and CD20  
481 (magenta) in the mammary gland of intact males (**a**) and neutered males (**b**) and within the  
482 intralobular (**c**) and interlobular mammary stroma (**d**). (**e, f**) Bar graphs illustrating  
483 differences in the mean number of T- lymphocytes per mm<sup>2</sup> of mammary stroma in the  
484 intralobular and interlobular stroma of intact (**e**) and neutered males (**f**) + standard deviation  
485 (\*\*p< 0.01, N= 5 for intact males, N =9 for neutered males, using Wilcoxon signed-rank  
486 test). Dots represent individual sheep. Images representative of 5 (**a, c, d**) and 9 (**b**) biological  
487 repeats. All IHC shown with a haematoxylin counterstain. Scale bar = 100 µm (**a, b**); 50 µm  
488 (**c, d**).

489

490



492 **Figure 6: Mast cells abundance is significantly higher in intact males. (a-c)** Dual  
493 immunohistochemical staining for c-Kit (brown) and alpha-SMA (magenta) in the mammary  
494 gland of intact males (**a**) and neutered males (**b**). Arrows indicate positive staining for mast  
495 cells. (**c**) Mast cells are located in close proximity to blood vessels in the male ovine  
496 mammary gland. Arrows indicate positive mast cell staining. (**d, e**) Bar graphs illustrating  
497 differences in the mean number of mast cells per mm<sup>2</sup> of intralobular (**d**) and interlobular (**e**)  
498 stroma in intact and neutered males + standard deviation (\*p< 0.05, N= 6 for intact males, N  
499 =7 for neutered males, using Mann-Whitney U test). (**f, g**) Bar graphs illustrating differences  
500 in the mean number of mast cells per mm<sup>2</sup> of mammary stroma in the intralobular and  
501 interlobular stroma of intact (**f**) and neutered males (**g**) + standard deviation (\*p< 0.05, N= 6  
502 for intact males, N =7 for neutered males, using Wilcoxon signed-rank test). Dots represent  
503 individual sheep. Images representative of 6 (**a, c**) and 7 (**b**) biological repeats. All IHC  
504 shown with a haematoxylin counterstain. Scale bar = 50  $\mu$ m (**a, b**); 25  $\mu$ m (**c**).

505

506

507

508

509

510

511

512

513

514 **References**

- 515 Atwood, C.S., Hovey, R.C., Glover, J.P., Chepko, G., Ginsburg, E., Robison, W.G.,  
516 Vonderhaar, B.K., 2000. Progesterone induces side-branching of the ductal epithelium in the  
517 mammary glands of peripubertal mice. *Journal of Endocrinology* 167, 39–52.  
518 <https://doi.org/10.1677/joe.0.1670039>
- 519 Beaudry, K.L., Parsons, C.L.M., Ellis, S.E., Akers, R.M., 2016. Localization and quantitation  
520 of macrophages, mast cells, and eosinophils in the developing bovine mammary gland1.  
521 *Journal of Dairy Science* 99, 796–804. <https://doi.org/10.3168/jds.2015-9972>
- 522 Brisken, C., Park, S., Vass, T., Lydon, J.P., O’Malley, B.W., Weinberg, R.A., 1998. A  
523 paracrine role for the epithelial progesterone receptor in mammary gland development. *Proc  
524 Natl Acad Sci U S A* 95, 5076–5081.
- 525 Cardiff, R.D., Jindal, S., Treuting, P.M., Going, J.J., Gusterson, B., Thompson, H.J., 2018. 23  
526 - Mammary Gland, in: Treuting, P.M., Dintzis, S.M., Montine, K.S. (Eds.), *Comparative  
527 Anatomy and Histology* (Second Edition). Academic Press, San Diego, pp. 487–509.  
528 <https://doi.org/10.1016/B978-0-12-802900-8.00023-3>
- 529 Cardoso, F., Bartlett, J.M.S., Slaets, L., van Deurzen, C.H.M., van Leeuwen-Stok, E., Porter,  
530 P., Linderholm, B., Hedenfalk, I., Schröder, C., Martens, J., Bayani, J., van Asperen, C.,  
531 Murray, M., Hudis, C., Middleton, L., Vermeij, J., Punie, K., Fraser, J., Nowaczyk, M.,  
532 Rubio, I.T., Aebi, S., Kelly, C., Ruddy, K.J., Winer, E., Nilsson, C., Lago, L.D., Korde, L.,  
533 Benstead, K., Bogler, O., Goulioti, T., Peric, A., Litière, S., Aalders, K.C., Poncet, C.,  
534 Tryfonidis, K., Giordano, S.H., 2018. Characterization of male breast cancer: results of the  
535 EORTC 10085/TBCRC/BIG/NABCG International Male Breast Cancer Program. *Annals of  
536 Oncology*, Incorporating blood-based liquid biopsy information into cancer staging 29, 405–  
537 417. <https://doi.org/10.1093/annonc/mdx651>

- 538 Chatterji, S., Krzoska, E., Thoroughgood, C.W., Saganty, J., Liu, P., Elsberger, B., Abu-Eid,  
539 R., Speirs, V., 2023. Defining genomic, transcriptomic, proteomic, epigenetic, and phenotypic  
540 biomarkers with prognostic capability in male breast cancer: a systematic review. *The Lancet  
541 Oncology* 24, e74–e85. [https://doi.org/10.1016/S1470-2045\(22\)00633-7](https://doi.org/10.1016/S1470-2045(22)00633-7)
- 542 Chen, W., Beck, I., Schober, W., Brockow, K., Effner, R., Buters, J.T.M., Behrendt, H., Ring,  
543 J., 2010. Human mast cells express androgen receptors but treatment with testosterone exerts  
544 no influence on IgE-independent mast cell degranulation elicited by neuromuscular blocking  
545 agents. *Experimental Dermatology* 19, 302–304. [https://doi.org/10.1111/j.1600-0625.2009.00969.x](https://doi.org/10.1111/j.1600-<br/>546 0625.2009.00969.x)
- 547 Chua, A.C.L., Hodson, L.J., Moldenhauer, L.M., Robertson, S.A., Ingman, W.V., 2010. Dual  
548 roles for macrophages in ovarian cycle-associated development and remodelling of the  
549 mammary gland epithelium. *Development* 137, 4229–4238.  
550 <https://doi.org/10.1242/dev.059261>
- 551 Colitti, M., Parillo, F., 2013. Immunolocalization of estrogen and progesterone receptors in  
552 ewe mammary glands. *Microscopy Research and Technique* 76, 955–962.  
553 <https://doi.org/10.1002/jemt.22254>
- 554 Dawson, C.A., Pal, B., Vaillant, F., Gandolfo, L.C., Liu, Z., Bleriot, C., Ginhoux, F., Smyth,  
555 G.K., Lindeman, G.J., Mueller, S.N., Rios, A.C., Visvader, J.E., 2020. Tissue-resident ductal  
556 macrophages survey the mammary epithelium and facilitate tissue remodelling. *Nat Cell Biol*  
557 22, 546–558. <https://doi.org/10.1038/s41556-020-0505-0>
- 558 Dimitrakakis, C., Bondy, C., 2009. Androgens and the breast. *Breast Cancer Research* 11,  
559 212. <https://doi.org/10.1186/bcr2413>

- 560 Drews, Ulrich, Drews, Ute, 1977. Regression of mouse mammary gland anlagen in  
561 recombinants of Tfm and wild-type tissues: testosterone acts via the mesenchyme. *Cell* 10,  
562 401–404. [https://doi.org/10.1016/0092-8674\(77\)90027-7](https://doi.org/10.1016/0092-8674(77)90027-7)
- 563 Dürnberger, H., Kratochwil, K., 1980. Specificity of tissue interaction and origin of  
564 mesenchymal cells in the androgen response of the embryonic mammary gland. *Cell* 19, 465–  
565 471. [https://doi.org/10.1016/0092-8674\(80\)90521-8](https://doi.org/10.1016/0092-8674(80)90521-8)
- 566 Fox, S., Speirs, V., Shaaban, A.M., 2022. Male breast cancer: an update. *Virchows Arch* 480,  
567 85–93. <https://doi.org/10.1007/s00428-021-03190-7>
- 568 Gao, Y.R. (Ellen), Walters, K.A., Desai, R., Zhou, H., Handelsman, D.J., Simanainen, U.,  
569 2014. Androgen Receptor Inactivation Resulted in Acceleration in Pubertal Mammary Gland  
570 Growth, Upregulation of ER $\alpha$  Expression, and Wnt/ $\beta$ -Catenin Signaling in Female Mice.  
571 *Endocrinology* 155, 4951–4963. <https://doi.org/10.1210/en.2014-1226>
- 572 Hassiotou, F., Geddes, D., 2013. Anatomy of the human mammary gland: Current status of  
573 knowledge. *Clin. Anat.* 26, 29–48. <https://doi.org/10.1002/ca.22165>
- 574 Hilton, H.N., Graham, J.D., Clarke, C.L., 2015. Minireview: Progesterone Regulation of  
575 Proliferation in the Normal Human Breast and in Breast Cancer: A Tale of Two Scenarios?  
576 *Molecular Endocrinology* 29, 1230–1242. <https://doi.org/10.1210/me.2015-1152>
- 577 Hodson, L.J., Chua, A.C.L., Evdokiou, A., Robertson, S.A., Ingman, W.V., 2013. Macrophage  
578 Phenotype in the Mammary Gland Fluctuates over the Course of the Estrous Cycle and Is  
579 Regulated by Ovarian Steroid Hormones1. *Biology of Reproduction* 89, 65, 1–8.  
580 <https://doi.org/10.1095/biolreprod.113.109561>

- 581 Hovey, R.C., Mcfadden, T.B., Akers, R.M., 1999. Regulation of Mammary Gland Growth  
582 and Morphogenesis by the Mammary Fat Pad: A Species Comparison. *J Mammary Gland  
583 Biol Neoplasia* 4, 53–68. <https://doi.org/10.1023/A:1018704603426>
- 584 Hughes, K., 2023. Studying Mammary Physiology and Pathology in Domestic Species  
585 Benefits Both Humans and Animals. *J Mammary Gland Biol Neoplasia* 28, 18.  
586 <https://doi.org/10.1007/s10911-023-09547-9>
- 587 Hughes, K., 2021a. Development and Pathology of the Equine Mammary Gland. *J Mammary  
588 Gland Biol Neoplasia* 26, 121–134. <https://doi.org/10.1007/s10911-020-09471-2>
- 589 Hughes, K., 2021b. Comparative mammary gland postnatal development and tumourigenesis  
590 in the sheep, cow, cat and rabbit: Exploring the menagerie. *Semin Cell Dev Biol* 114, 186–  
591 195. <https://doi.org/10.1016/j.semcdb.2020.09.010>
- 592 Hughes, K., Watson, C.J., 2018. The Mammary Microenvironment in Mastitis in Humans,  
593 Dairy Ruminants, Rabbits and Rodents: A One Health Focus. *J Mammary Gland Biol  
594 Neoplasia* 23, 27–41. <https://doi.org/10.1007/s10911-018-9395-1>
- 595 Hughes, K., Wickenden, J.A., Allen, J.E., Watson, C.J., 2012. Conditional deletion of Stat3 in  
596 mammary epithelium impairs the acute phase response and modulates immune cell numbers  
597 during post-lactational regression. *The Journal of Pathology* 227, 106–117.  
598 <https://doi.org/10.1002/path.3961>
- 599 Inman, J.L., Robertson, C., Mott, J.D., Bissell, M.J., 2015. Mammary gland development:  
600 cell fate specification, stem cells and the microenvironment. *Development* 142, 1028–1042.  
601 <https://doi.org/10.1242/dev.087643>
- 602 Iuanow, E., Kettler, M., Slanetz, P.J., 2011. Spectrum of Disease in the Male Breast.  
603 *American Journal of Roentgenology* 196, W247–W259. <https://doi.org/10.2214/AJR.09.3994>

- 604 Jenkinson, C.M.C., 2003. The pattern and regulation of mammary gland development during  
605 fetal life in sheep : a thesis presented in partial fulfilment of the requirements for the degree  
606 of Doctor of Philosophy in Animal Science at Massey University, Palmerston North, New  
607 Zealand. Massey University.
- 608 Jesinger, R.A., 2014. Breast Anatomy for the Interventionalist. Techniques in Vascular and  
609 Interventional Radiology, Breast Interventions 17, 3–9.  
610 <https://doi.org/10.1053/j.tvir.2013.12.002>
- 611 Kolla, S., Pokharel, A., Vandenberg, L.N., 2017. The mouse mammary gland as a sentinel  
612 organ: distinguishing ‘control’ populations with diverse environmental histories. Environ  
613 Health 16, 25. <https://doi.org/10.1186/s12940-017-0229-1>
- 614 Lammie, A., Drobniak, M., Gerald, W., Saad, A., Cote, R., Cordon-Cardo, C., 1994.  
615 Expression of c-kit and kit ligand proteins in normal human tissues. Journal of  
616 Histochemistry & Cytochemistry 42, 1417–1425. <https://doi.org/10.1177/42.11.7523489>
- 617 Lilla, J.N., Werb, Z., 2010. Mast cells contribute to the stromal microenvironment in  
618 mammary gland branching morphogenesis. Developmental Biology 337, 124–133.  
619 <https://doi.org/10.1016/j.ydbio.2009.10.021>
- 620 Liu, N., Johnson, K.J., Ma, C.X., 2018. Male Breast Cancer: An Updated Surveillance,  
621 Epidemiology, and End Results Data Analysis. Clinical Breast Cancer 18, e997–e1002.  
622 <https://doi.org/10.1016/j.clbc.2018.06.013>
- 623 Liva, S.M., Voskuhl, R.R., 2001. Testosterone Acts Directly on CD4+ T Lymphocytes to  
624 Increase IL-10 Production1. The Journal of Immunology 167, 2060–2067.  
625 <https://doi.org/10.4049/jimmunol.167.4.2060>

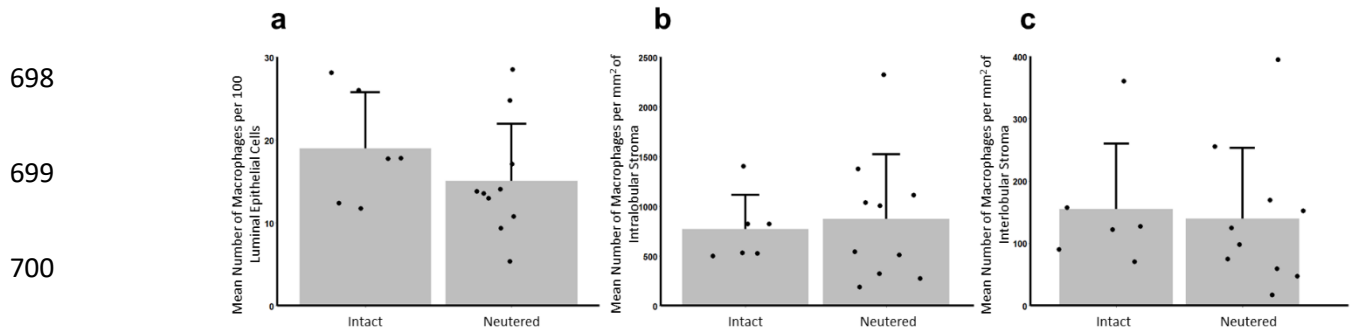
- 626 Lloyd-Lewis, B., Davis, F.M., Harris, O.B., Hitchcock, J.R., Lourenco, F.C., Pasche, M.,
- 627 Watson, C.J., 2016. Imaging the mammary gland and mammary tumours in 3D: optical tissue
- 628 clearing and immunofluorescence methods. *Breast Cancer Research* 18, 127.
- 629 <https://doi.org/10.1186/s13058-016-0754-9>
- 630 Macias, H., Hinck, L., 2012. Mammary gland development. *WIREs Developmental Biology*
- 631 1, 533–557. <https://doi.org/10.1002/wdev.35>
- 632 Morrison, J., Berry, M., Botting, K., Darby, J., Frasch, M., Gatford, K., Giussani, D., Gray,
- 633 C., Harding, R., Herrera, E., Kemp, M., Lock, M., Mcmillen, I., Moss, T., Musk, G., Oliver,
- 634 M., Regnault, T., Roberts, C., Soo, J., Tellam, R., 2018. Improving pregnancy outcomes in
- 635 humans through studies in sheep. *American Journal of Physiology-Regulatory, Integrative*
- 636 and *Comparative Physiology* 315. <https://doi.org/10.1152/ajpregu.00391.2017>
- 637 Nagy, D., Gillis, C.M.C., Davies, K., Fowden, A.L., Rees, P., Wills, J.W., Hughes, K., 2021.
- 638 Developing ovine mammary terminal duct lobular units have a dynamic mucosal and stromal
- 639 immune microenvironment. *Commun Biol* 4, 993. <https://doi.org/10.1038/s42003-021-02502-6>
- 641 Newman, S.J., Smith, S.A., Zimmerman, K., 2021. Mammary carcinoma arising in an
- 642 adenoma in a ewe. *J Vet Diagn Invest* 33, 566–571.
- 643 <https://doi.org/10.1177/1040638721993061>
- 644 Paine, I.S., Lewis, M.T., 2017. The Terminal End Bud: the Little Engine that Could. *J*
- 645 *Mammary Gland Biol Neoplasia* 22, 93–108. <https://doi.org/10.1007/s10911-017-9372-0>
- 646 Pokharel, A., Kolla, S., Matouskova, K., Vandenberg, L.N., 2018. Asymmetric development
- 647 of the male mouse mammary gland and its response to a prenatal or postnatal estrogen
- 648 challenge. *Reprod Toxicol* 82, 63–71. <https://doi.org/10.1016/j.reprotox.2018.10.003>

- 649 Ramirez, R.A., Lee, A., Schedin, P., Russell, J.S., Masso-Welch, P.A., 2012. Alterations in  
650 mast cell frequency and relationship to angiogenesis in the rat mammary gland during  
651 windows of physiologic tissue remodeling. *Developmental Dynamics* 241, 890–900.  
652 <https://doi.org/10.1002/dvdy.23778>
- 653 Renfree, M.B., Robinson, E.S., Short, R.V., Vandeberg, J.L., 1990. Mammary glands in male  
654 marsupials: I. Primordia in neonatal opossums *Didelphis virginiana* and *Monodelphis*  
655 *domestica*. *Development* 110, 385–390. <https://doi.org/10.1242/dev.110.2.385>
- 656 Ribatti, D., 2018. The Staining of Mast Cells: A Historical Overview. *International Archives*  
657 of Allergy and Immunology
- 658 176, 55–60. <https://doi.org/10.1159/000487538>
- 659 Richert, M.M., Schwertfeger, K.L., Ryder, J.W., Anderson, S.M., 2000. An Atlas of Mouse  
660 Mammary Gland Development. *J Mammary Gland Biol Neoplasia* 5, 227–241.  
<https://doi.org/10.1023/A:1026499523505>
- 661 Rowson, A.R., Daniels, K.M., Ellis, S.E., Hovey, R.C., 2012. Growth and development of the  
662 mammary glands of livestock: A veritable barnyard of opportunities. *Seminars in Cell &*  
663 *Developmental Biology, Cell Regulation by Selective Protein Degradation & Biology of*  
664 *Mammary Gland Development* 23, 557–566. <https://doi.org/10.1016/j.semcd.2012.03.018>
- 665 Safayi, S., Korn, N., Bertram, A., Akers, R.M., Capuco, A.V., Pratt, S.L., Ellis, S., 2012.  
666 Myoepithelial cell differentiation markers in prepubertal bovine mammary gland: Effect of  
667 ovariectomy. *Journal of Dairy Science* 95, 2965–2976. <https://doi.org/10.3168/jds.2011-4690>
- 668 Schindelin, J., Arganda-Carreras, I., Frise, E., Kaynig, V., Longair, M., Pietzsch, T., Preibisch,  
669 S., Rueden, C., Saalfeld, S., Schmid, B., Tinevez, J.-Y., White, D.J., Hartenstein, V., Eliceiri,  
670 K., Tomancak, P., Cardona, A., 2012. Fiji: an open-source platform for biological-image  
671 analysis. *Nature Methods* 9, 676–682. <https://doi.org/10.1038/nmeth.2019>

- 672 Simanainen, U., Gao, Y.R., Walters, K.A., Watson, G., Desai, R., Jimenez, M., Handelsman,  
673 D.J., 2012. Androgen Resistance in Female Mice Increases Susceptibility to DMBA-Induced  
674 Mammary Tumors. *Hormones and Cancer* 3, 113–124. <https://doi.org/10.1007/s12672-012-0107-9>
- 676 Stewart, T.A., Hughes, K., Hume, D.A., Davis, F.M., 2019. Developmental Stage-Specific  
677 Distribution of Macrophages in Mouse Mammary Gland. *Frontiers in Cell and*  
678 *Developmental Biology* 7, 250. <https://doi.org/10.3389/fcell.2019.00250>
- 679 Susaki, E.A., Tainaka, K., Perrin, D., Kishino, F., Tawara, T., Watanabe, T.M., Yokoyama, C.,  
680 Onoe, H., Eguchi, M., Yamaguchi, S., Abe, T., Kiyonari, H., Shimizu, Y., Miyawaki, A.,  
681 Yokota, H., Ueda, H.R., 2014. Whole-Brain Imaging with Single-Cell Resolution Using  
682 Chemical Cocktails and Computational Analysis. *Cell* 157, 726–739.  
683 <https://doi.org/10.1016/j.cell.2014.03.042>
- 684 Szabo, G.K., Vandenberg, L.N., 2021. REPRODUCTIVE TOXICOLOGY: The male  
685 mammary gland: a novel target of endocrine-disrupting chemicals. *Reproduction* 162, F79–  
686 F89. <https://doi.org/10.1530/REP-20-0615>
- 687 Tower, H., Dall, G., Davey, A., Stewart, M., Lanteri, P., Ruppert, M., Lambouras, M., Nasir,  
688 I., Yeow, S., Darcy, P.K., Ingman, W.V., Parker, B., Haynes, N.M., Britt, K.L., 2022.  
689 Estrogen-induced immune changes within the normal mammary gland. *Scientific Reports* 12,  
690 18986. <https://doi.org/10.1038/s41598-022-21871-4>
- 691 Vandenberg, L.N., Schaeberle, C.M., Rubin, B.S., Sonnenschein, C., Soto, A.M., 2013. The  
692 male mammary gland: A target for the xenoestrogen bisphenol A. *Reproductive Toxicology*  
693 37, 15–23. <https://doi.org/10.1016/j.reprotox.2013.01.002>
- 694
- 695

696 **Supplementary Material**

697

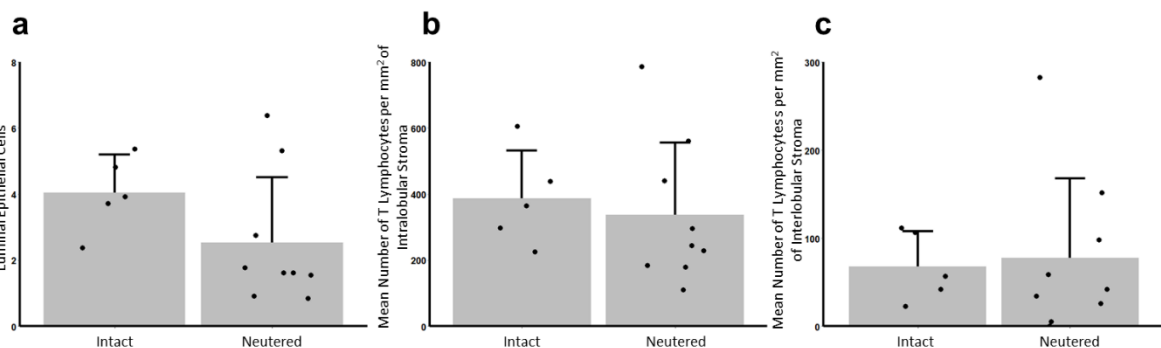


702 Supplementary Figure 1: There is no significant difference in macrophage abundance in the  
703 mammary glands of intact and neutered males. (a- c) Bar graphs illustrating differences,  
704 between intact and neutered males, in the mean number of macrophages per 100 luminal  
705 epithelial cells (a) and the mean number of macrophages per mm<sup>2</sup> of intralobular (b) or  
706 interlobular (c) + standard deviation (N= 6 for intact males, N =10 for neutered males, using  
707 Mann-Whitney U test). Dots represent individual sheep.

708

709

710

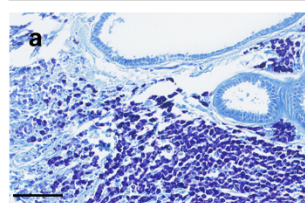


711

712  
713  
714  
715 Supplementary Figure 2: There is no significant difference in T-lymphocyte abundance in the  
716 mammary glands of intact and neutered males. (a- c) Bar graphs illustrating differences,  
717 between intact and neutered males, in the mean number of T-lymphocytes per 100 luminal  
718 epithelial cells (a) and the mean number of T-lymphocytes per mm<sup>2</sup> of intralobular (b) or  
719 interlobular (c) + standard deviation (N= 5 for intact males, N =9 for neutered males, using  
720 Mann-Whitney U test). Dots represent individual sheep.

721

Positive Control Tissue  
(Mast Cell Tumour)

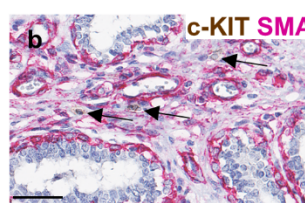


722

723

724

Immunohistochemical  
Staining (c-KIT)



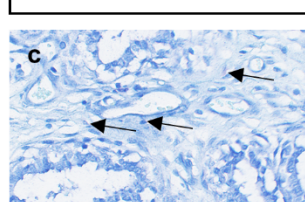
725

726

727

728

Toluidine Blue Staining



729

730

731 Supplementary Figure 3: Toluidine blue staining does not positively stain mast cells in the  
732 ovine mammary gland. (a) Toluidine blue staining in a positive control tissue, a mast cell  
733 tumour. (b, c) Sequentially cut sections of FFPE ovine mammary gland tissue. (b) Dual  
734 immunohistochemical staining for c-Kit and alpha-SMA. Arrows indicate positive staining  
735 for mast cells. (c) Toluidine blue staining. Arrows indicate areas where positive toluidine  
736 staining should be. Images representative of 3 biological repeats. All IHC shown with a  
737 haematoxylin counterstain. Scale bar = 100  $\mu$ m (a); 50  $\mu$ m (b, c).

738

739

740 Supplementary Table 1: Full details of sheep used in the study.

Sheep i.d.	Sex	Source	Age	Breed	UK Meteorological		Staining
					Season	Died/Euthanised	
L44	Male	Diagnostic PM	7 weeks	Mule Cross	Spring	Intact	CUBIC (SMA), CUBIC (IBA1/SMA)
L45	Male	Research	3 days	Welsh Mountain	Spring	Intact	CUBIC (SMA), CUBIC (IBA1/SMA)
S84	Male	Research	Mature (2 years +)	Welsh Mountain	Winter	Intact	Ki67/SMA, AR/SMA, ER/SMA, PR/SMA, IBA1/SMA, CD3/CD20, cKit/SMA
S131	Male	Diagnostic PM	6 months	Shetland	Summer	Neutered	Ki67/SMA, AR/SMA, ER/SMA, PR/SMA, IBA1/SMA, CD3/CD20, cKit/SMA
S132	Male	Diagnostic PM	Mature (2 years +)	Unknown	Autumn	Intact	Ki67/SMA, AR/SMA, ER/SMA, PR/SMA, IBA1/SMA, CD3/CD20, cKit/SMA
S133	Male	Diagnostic PM	9 months	Unknown	Winter	Neutered	IBA1/SMA
S154	Male	Diagnostic PM	Mature (2 years +)	Unknown	Spring	Intact	Ki67/SMA, AR/SMA, ER/SMA, PR/SMA, IBA1/SMA, CD3/CD20, cKit/SMA
P20/97	Male	Diagnostic PM	4 months	Mule	Summer	Neutered	Ki67/SMA, AR/SMA, ER/SMA, PR/SMA, IBA1/SMA, CD3/CD20, cKit/SMA
P20/154	Male	Diagnostic PM	Mature (3 years)	Suffolk	Autumn	Intact	Ki67/SMA, IBA1/SMA, cKit/SMA
P21/357	Male	Diagnostic PM	8 months	Cheviot Cross	Autumn	Neutered	Ki67/SMA, AR/SMA, ER/SMA, PR/SMA, IBA1/SMA, CD3/CD20, cKit/SMA
P21/358	Male	Diagnostic PM	8 months	New Zealand Romney	Autumn	Neutered	Ki67/SMA, AR/SMA, ER/SMA, PR/SMA, IBA1/SMA, CD3/CD20, cKit/SMA
P21/366	Male	Diagnostic PM	9 months	Cheviot Cross	Winter	Neutered	Ki67/SMA, AR/SMA, ER/SMA, PR/SMA, IBA1/SMA, CD3/CD20, cKit/SMA
P21/367	Male	Diagnostic PM	10 months	Cheviot Cross	Winter	Neutered	Ki67/SMA, AR/SMA, ER/SMA, PR/SMA, IBA1/SMA, CD3/CD20, cKit/SMA
P21/369	Male	Diagnostic PM	11 months	Cheviot Cross	Winter	Neutered	Ki67/SMA, AR/SMA, ER/SMA, PR/SMA, IBA1/SMA, CD3/CD20
P22/66	Male	Diagnostic PM	14 months	Welsh Mountain	Spring	Intact	Ki67/SMA, AR/SMA, ER/SMA, PR/SMA, IBA1/SMA, CD3/CD20, cKit/SMA
P22/27	Male	Diagnostic PM	8 months	Texel Cross	Winter	Neutered	Ki67/SMA, AR/SMA, ER/SMA, PR/SMA, IBA1/SMA, CD3/CD20, cKit/SMA
P22/233	Male	Diagnostic PM	5 months	Texel Cross	Autumn	Intact	Ki67/SMA, AR/SMA, ER/SMA, PR/SMA, IBA1/SMA, CD3/CD20, cKit/SMA
P23/130	Male	Diagnostic PM	7 weeks	Texel Cross	Spring	Neutered	CUBIC (SMA), CUBIC (IBA1/SMA)
P23/133	Male	Diagnostic PM	Mature (2 years +)	Jacob Cross	Spring	Neutered	Ki67/SMA, AR/SMA, ER/SMA, PR/SMA, IBA1/SMA, CD3/CD20
P16 138	Female	Diagnostic PM	5 months	Texel Cross	Summer	Intact	Ki67/SMA, AR/SMA, ER/SMA, PR/SMA
P18 247	Female	Diagnostic PM	4 months	Beltex	Autumn	Intact	Ki67/SMA, AR/SMA, ER/SMA, PR/SMA
S43	Female	Research	8 months	Welsh Mountain	Winter	Intact	Ki67/SMA, AR/SMA, ER/SMA, PR/SMA
S44	Female	Research	11 months	Welsh Mountain	Winter	Intact	Ki67/SMA, AR/SMA, ER/SMA, PR/SMA
S47	Female	Research	9 months	Welsh Mountain	Winter	Intact	Ki67/SMA, AR/SMA, ER/SMA, PR/SMA
S52	Female	Research	9 months	Welsh Mountain	Spring	Intact	Ki67/SMA, AR/SMA, ER/SMA, PR/SMA
S78	Female	Research	11 months	Welsh Mountain	Autumn	Intact	Ki67/SMA, AR/SMA, ER/SMA, PR/SMA
S141	Female	Research	Mature (2 years +)	Mountain	Summer	Intact	Ki67/SMA, AR/SMA, ER/SMA, PR/SMA
S142	Female	Research	Mature (2 years +)	Welsh Mountain	Summer	Intact	Ki67/SMA, AR/SMA, ER/SMA, PR/SMA

S143	Female	Research	Mature (2 years +)	Welsh Mountain	Summer	Intact	Ki67/SMA, AR/SMA, ER/SMA, PR/SMA
S144	Female	Research	Mature (2 years +)	Welsh Mountain	Summer	Intact	Ki67/SMA, AR/SMA, ER/SMA, PR/SMA
S145	Female	Research	Mature (2 years +)	Welsh Mountain	Summer	Intact	Ki67/SMA, AR/SMA, ER/SMA, PR/SMA
S146	Female	Research	Mature (2 years +)	Welsh Mountain	Summer	Intact	Ki67/SMA, AR/SMA, ER/SMA, PR/SMA
S147	Female	Research	Mature (2 years +)	Welsh Mountain	Summer	Intact	Ki67/SMA, AR/SMA, ER/SMA, PR/SMA

741

742

743 Supplementary Table 2: Full details of primary and secondary antibodies utilised in  
 744 immunohistochemical, immunofluorescence and CUBIC staining.

Target	Application (IHC, immunohistochemistry; IF, immunofluorescence; CUBIC, 3D tissue clearing)	Species and Clone (where stated)	Dilution	Manufacturer	Catalogue number
<i>Primary antibodies</i>					
E-cadherin	IF	Mouse monoclonal anti-human [NCH-38]	1:100	Dako/Agilent	M3612
Alpha Smooth muscle actin	Dual colour IHC, CUBIC	Mouse monoclonal anti-human [1A4]	1:500 (dual colour IHC), 1:100 (CUBIC)	Dako/Agilent	M0851
Alpha Smooth muscle actin	Dual colour IHC, IF	Rabbit monoclonal [EPR5368]	1:2000	Abcam	Ab124964
Ki67	Dual colour IHC	Mouse monoclonal anti-human [MIB-1]	1:100	Dako/Agilent	M7240
Androgen Receptor	IF	Rabbit monoclonal [EPR1535(2)]	1:100	Abcam	Ab133273
Oestrogen Receptor $\alpha$	IF	Rabbit monoclonal [D6R2W]	1:200	Cell Signalling Technology	13258S
Progesterone Receptor A/B	IF	Rabbit monoclonal [D8Q2J]	1:1000	Cell Signalling Technology	8757S
IBA1	Dual colour IHC, CUBIC	Rabbit monoclonal [EPR16588]	1:1200 (dual colour IHC), 1:400 (CUBIC)	Abcam	Ab178846
CD3	Dual colour IHC	Mouse monoclonal [F7.2.38]	1:250	Dako/Agilent	M7254
CD20	Dual colour IHC	Rabbit monoclonal [E7B7T]	1:500	Cell Signalling Technology	48750S
c-Kit	Dual colour IHC	Rabbit monoclonal [D3W6Y]	1:100	Cell Signalling Technology	37805S
<i>Secondary antibodies</i>					
Mouse IgG, Alexa Fluor Plus 488	IF, CUBIC	Goat	1:500	Thermo Fisher Scientific	A32723
Rabbit IgG, Alexa Fluor Plus 647	IF, CUBIC	Goat	1:500	Thermo Fisher Scientific	A32733

745